Available online at www.sciencedirect.com
ScienceDirect
Journal of Nuclear Materials 376 (2008) 66–77
journal of nuclear materials
www.elsevier.com/locate/jnucmat

Comparison of interatomic potentials for UO_2 Part II: Molecular dynamics simulations

K. Govers [a,b,*], S. Lemehov [b], M. Hou [c], M. Verwerft [b]

[a] Service de Métrologie Nucléaire (CP 165/84), Université Libre de Bruxelles, 50 av. F.D. Roosevelt, B-1050 Bruxelles, Belgium
[b] Institute for Nuclear Materials Science, SCK-CEN, Boeretang 200, B-2400 Mol, Belgium
[c] Physique des Solides Irradiés et des Nanostructures (CP 234), Université Libre de Bruxelles, Bd du Triomphe, B-1050 Bruxelles, Belgium

Received 10 April 2007; accepted 16 January 2008

Abstract

An improved knowledge of nuclear fuel can be gained from a better description of atomic-scale processes such as point defects behaviour under irradiation. In these perspectives, computer simulation techniques involving semi-empirical potentials can play a major role as they allow studying some of these processes separately. The range of applicability in static calculations of the available interatomic potentials for UO_2 has been previously assessed by the authors. This study complements the static calculations by including dynamical simulations of the temperature evolution of different elastic properties (lattice parameter, specific heat, bulk modulus and Gruneisen parameter) and by calculations of bulk melting temperature.

PACS: 31.15.Qg; 34.20.Cf; 61.72.−y; 61.72.Ji; 66.30.Hs; 71.15.Pd; 83.10.Rp

1. Introduction

The evolution of the nuclear fuel, under irradiation or in storage repository, is affected by many phenomena that cannot always be isolated experimentally. Computer simulations are a way to avoid such complications, as isolated processes can be simulated. Techniques involving interatomic potentials are in this context very promising. They allow determining structure information, such as defect properties working at 0 K with a limited number of atoms, but they can also be used to determine the evolution of a larger system under different conditions of pressure, volume or temperature.

In a previous article [1] we already estimated the range of applicability of the different potentials developed for UO_2 using static calculations. We could determine various elastic and defect properties, at zero temperature. With this article, we will complete this study including the dynamical behaviour of UO_2. Molecular dynamics simulations have been performed under different conditions of temperature and volume in order to analyze the temperature evolution of several thermodynamic properties up to 3000 K: lattice parameter, specific heat, bulk modulus and Gruneisen parameter. The second stage of this study was the analysis of the predicted melting temperature. For computation time reasons, shell–core MD being about ten times slower than MD with rigid ion potentials, this stage was only performed for five rigid ion potentials: *Basak*, *Karakasidis*, *Morelon*, *Walker*, *Yamada*. For clarity, rigid ion potentials will be written in italic, shell–core potentials in bold in the text; on the figures, crosses will be used for rigid ion potentials with non-formal charges, open symbols for rigid ion potentials with formal charges and full symbols for shell–core potentials.

* Corresponding author. Address: Institute for Nuclear Materials Science, SCK-CEN, Boeretang 200, B-2400 Mol, Belgium.
E-mail address: kgovers@sckcen.be (K. Govers).

0022-3115/$ - see front matter © 2008 Elsevier B.V. All rights reserved.
doi:10.1016/j.jnucmat.2008.01.023

2. Calculation technique

2.1. Interatomic potentials

A molecular dynamics (MD) simulation allows determining the time-evolution of a system of atoms. In order to perform such a simulation the forces acting on each atom are derived from an effective interatomic potential, describing in a simple way atomic interactions. The same formalism is used in energy minimisation techniques (cf. the first part of this work [1]) but in that case the interatomic potential serves to find configurations presenting a local minimum of energy.

Two models accounting for atomic description have been considered by the different authors having developed potentials for UO_2 [2–16]. The first one is the rigid ion model, which describes atoms as massive point charges interacting by electrostatic interactions and a short-range potential. The second model is the shell–core model [17] which describes atoms as one massive point charge – representing the nucleus and the inner electron shells – bound by a spring to a massless shell – representing the valence electron shell. In this model the electrostatic interactions act between both species, but the short-range potential acts between shells only. With both models, interactions between ions have been formulated in terms of a short-range potential in addition to the long-range coulombic interactions. Three different forms of short-range potentials have been used by these authors: Buckingham, Buckingham-4-ranges and Buckingham + Morse potentials.

The most used was the Buckingham potential

$$V_{ij}(r) = A_{ij}\exp\left(-\frac{r}{\rho_{ij}}\right) - \frac{C_{ij}}{r^6}, \tag{1}$$

where r is the distance between atoms i and j. The Buckingham form yields unphysical attraction at very short distance because of the $1/r^6$ term. This zone is separated from the 'conventional' zone by an energy barrier whose location and height depends on the potential parameters. These short distances being potentially reached in MD runs at high temperature, care has to be taken in order to avoid entering this unphysical zone.

The problem of entering the unphysical region appeared in some of our simulations – with the following potentials: **Catlow1**, **Catlow2**, **Jackson1**, **Jackson2**, *Karakasidis*, *Lewis_a*, **Meis2**, *Sindzingre*, *Tharmalingam1*, *Walker* – at higher than they were initially developed for. To overcome this problem, we 'hardened' the potentials by the addition of a strong repulsive term at very short distance to the O–O and/or O–U interactions of the problematic potentials, with the form

$$V_{\text{repuls}}(r) = A\cdot\exp\left(\frac{r}{\rho}\right) \tag{2}$$

where we used the following values: $A = 1.0\times10^{12}$ eV and $\rho = 0.06$ Å. This additional term provides a sufficiently high energy barrier at small separation and, at the same time, does not affect the potential at 'normal' distances (see Fig. 1), in perfect lattice and defect configurations. This has been checked by repeating the static calculations of lattice parameter, elastic constants and defect properties with the modified potential. Less than 1% difference with the original potential predictions (see [1]) was observed.

An interesting point to note is that previous authors [9,18] made simulations at high temperatures with the *Karakasidis* and **Jackson2** potentials and did not encounter this problem. It has been suggested by Karakasidis [19] that a too large timestep or a too low number of reciprocal-space vectors used in the Ewald summation can be responsible for it, but modifications of these parameters did not result in any improvement of our simulations.

Different authors avoided this problem during the potential development using a 'Buckingham-4 ranges' potential, defined by intervals

$$V_{ij}(r) = \begin{cases} A_{ij}\exp\left(-\frac{r}{\rho_{ij}}\right) & \text{if } r \leqslant r_1, \\ \text{5th-degree polynomial} & \text{if } r_1 < r \leqslant r_{\min}, \\ \text{3rd-degree polynomial} & \text{if } r_{\min} < r \leqslant r_2, \\ -\frac{C_{ij}}{r^6} & \text{if } r > r_2. \end{cases} \tag{3}$$

The two splines are such that the potential and its two first derivatives are continuous and that $r_{\min}$ is the potential minimum. This form was used only for the O–O interactions, and the above-mentioned hardening of potential had in some cases (**Jackson1**, **Jackson2**, *Karakasidis*, *Sindzingre*, *Walker*) to be done for the O–U interactions.

The last form of potential found in MD simulations of UO_2, consists into the addition of a Morse potential, used in order to describe a covalent bond, to a Buckingham potential. A partial ionization is generally assumed with such a model. The potential is expressed by

$$V_{ij}(r) = f_0(b_i+b_j)\exp\left(\frac{a_i+a_j-r}{b_i+b_j}\right) - \frac{c_ic_j}{r^6} + D_{ij}\left\{\left[1-\exp\left(\beta_{ij}(r-r^*_{ij})\right)\right]^2 - 1\right\} \tag{4}$$

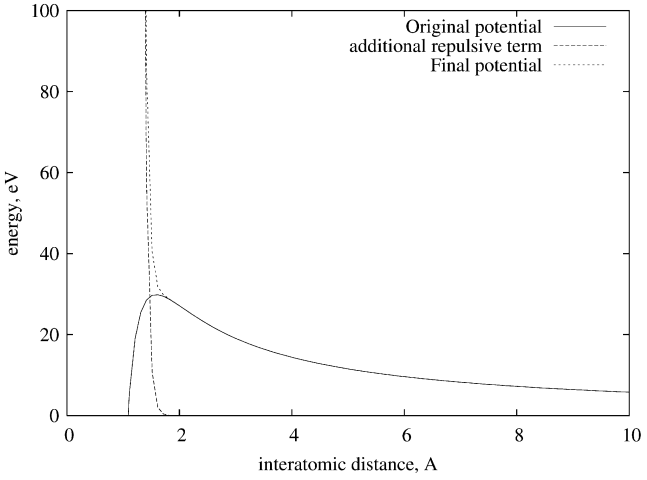

Fig. 1. Addition of a repulsive term to the O–O potential. The coulombic term is included in the potential function.

The parameters of the different potentials [2–16] have been reported in the first part of this work [1], and will not be repeated here. All short-range potentials were used in this work with a cut-off of 10.4 Å while the Coulomb interactions were treated with the classical Ewald summation technique.

2.2. Temperature evolution of different properties

MD simulations were used in order to evaluate the temperature evolution of different lattice properties predicted by the different potentials developed for UO_2. The simulations were done at constant volume and energy (NVE ensemble) with the GULP code [20] using a box of 768 atoms ($4 \times 4 \times 4$ conventional unit cells) which is sufficient, according to the convergence observed with other box sizes, in order to obtain reliable data. Periodic boundary conditions were applied in order to simulate an infinite crystal. It allows avoiding surface effects that would appear for the – inevitably small – system that can be considered in MD simulations.

The simulations were run at different temperature, varying from 100 K up to 3000 K, by steps of 100 K. The temperature was controlled by a temperature rescaling procedure during 1 ps, then the system was equilibrated during 4 ps. After this, the next 5 ps were used in order to calculate average values of volume, pressure, energy and temperature. The timestep used in all simulation was 1 fs.

At each temperature, and for each potential, 7 runs were performed using 7 different box sizes (chosen to be close to the 0 bar box size predicted by the potential under consideration). An interpolation of these results provides estimations of various lattice properties: lattice parameter ($a_0(T)$), isothermal bulk modulus ($B_T(T)$), specific heat ($c_p(T)$ and $c_V(T)$) and Gruneisen parameter ($\gamma(T)$). The following definitions were used

$$\begin{aligned} a_0(T) &= \sqrt[3]{V(T, p=0)} \\ B_T(T) &= -V(T)\left(\frac{\partial p}{\partial V}\right)_T \\ C_p(T) &= \left(\frac{\partial E}{\partial T}\right)_p \\ C_V(T) &= \left(\frac{\partial E}{\partial T}\right)_V \\ \gamma(T) &= V(T)\left(\frac{\partial p}{\partial E}\right)_T \end{aligned} \tag{5}$$

As it was said, the intention was to evaluate all the potentials in the NVE (microcanonical) ensemble, but a problem appeared with all the shell–core potentials: a rapid decrease of energy was observed while working in NVE ensemble (thus at constant energy!). Some tests showed that integrating the motion of the uranium atoms was problematic when a shell–core description of U atoms was used. Solutions like increasing the number of iterations used to calculate shells positions or decreasing the timestep have been tested. The energy drift was reduced but still present, and at the expense of computing time (up to 10 times slower). The second way to perform shell–core MD consists into attributing a small fraction of the ion mass to the shell, but it also requires smaller timesteps (of the order of 0.1 fs) and therefore longer simulations in order to sample correctly the shell motion. In this last case, energy could be conserved.

The solution envisaged was to couple the system to a Nosé thermostat for all runs with shell–core potentials, which preserved the computing time. The coupling to a thermostat does not imply that the extended hamiltonian will now be conserved, it is even expected that the same integration problem will appear again. The check of this could not be done since the extended hamiltonian is not a standard output of GULP.

It means that, even if the temperature of the runs are now controlled by a Nosé thermostat, the system evolution will not sample the NVT ensemble, but rather a pseudo-NVT (since the average temperature is still controlled), that we will denote $\mathrm{NV}\widetilde{\mathrm{T}}$. Nevertheless, assuming that ergodicity applies to our simulations, the average of any quantity calculated in, e.g., the NVE and the $\mathrm{NV}\widetilde{\mathrm{T}}$ ensemble will be the same in the thermodynamic limit of infinite system size, as long as E and $\widetilde{T}$ are consistent with each other ($\widetilde{T} = \langle T \rangle_{\mathrm{NVE}}$) [21]. This guarantees that our simulations provide reliable averages. It should, however, be noted that the fluctuations of e.g. energy obtained in our $\mathrm{NV}\widetilde{\mathrm{T}}$ will *not* be equivalent to the fluctuations in the NVT ensemble because of the non-conservation of the extended hamiltonian.

In order to show that ergodicity applies to our simulations, we performed a few MD runs, in the NVE ensemble under the same conditions as some of our $\mathrm{NV}\widetilde{\mathrm{T}}$ simulations, in which a small fraction of the ion mass was attributed to the electron shell.

The averages obtained in both ensemble were in excellent agreement since their variation ranges in the two methods were overlapping, which indicates our method is applicable.

2.3. Determination of the melting temperature

2.3.1. Generalities

The melting temperature was determined joining two 'boxes', the first one consisting of a solid UO_2 phase at a given temperature, the second one consisting of a liquid UO_2 phase at the same temperature. This liquid phase was obtained from a run at very high temperature – 22 000 K – in order to create an important disorder and then stabilized for a few ps at the same temperature as the solid phase. The initial configuration of the runs is shown on Fig. 2.

During the simulation, the separation surface between the liquid and solid phase will move. If the system energy is too low to maintain the liquid phase, the whole system

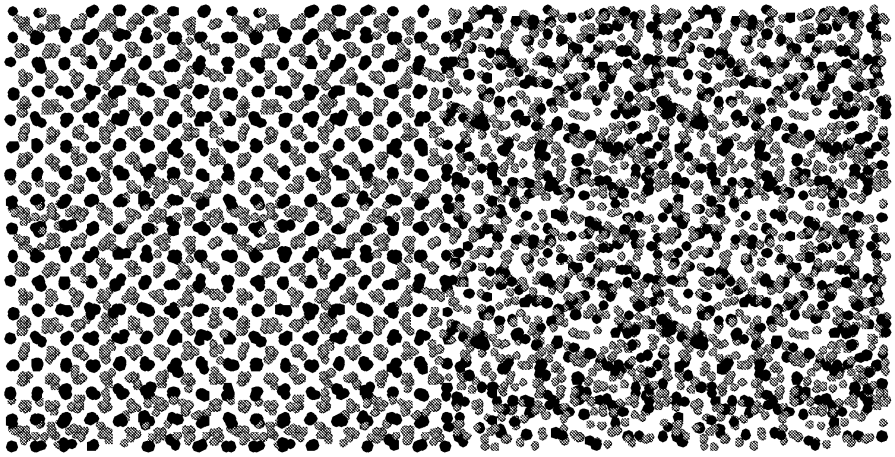

Fig. 2. Initial configuration of the run for the determination of the melting temperature. Picture obtained with the VMD program [22].

will become solid. Similarly, if the system energy is sufficiently high, the liquid phase will dominate. There is an energy range where the two phases can coexist (at least for a macroscopic system), the temperature being constant (and called the melting temperature). In that case the separation surface will move until equilibrium is reached. For the smallest systems considered here the separation surface was sometimes energetically costly (because split over a small number of atoms) and only one phase should be finally observed, if the simulation is long enough. Two techniques have been used to confirm the equilibrium of the system. The first one simply consists in the visualization of the atoms trajectory, the solid phase being easily identifiable. The stabilisation of the surfaces between the solid and liquid phases indicates that equilibrium is reached. The second technique considered in this work was to study the structure factor, or more precisely, its squared amplitude $|S'_\alpha(\vec{k})|^2$ for the U and O sublattices. We used the notation $\alpha =$ U or O sublattices; $\vec{k} =$ reciprocal vector of the fcc lattice. The structure factor is defined as

$$S(\vec{k}) = \sum_{n=1}^{N_{u.c.}} f_n \exp(i\vec{k}\cdot\vec{r_n}) \tag{6}$$

where the sum concerns all atoms in the unit cell, and f_n is the atomic scattering factor of atom n. In our study we will compute the amplitude of the structure factor for the whole system (i.e. not for a unit cell), considering the U and O sublattices separately. This quantity will be called $|S'_\alpha(\vec{k})|^2$, where α refers to the U or O atoms, and is defined in Eq. (7). It has been normalized in order to compare more easily systems of different sizes.

$$|S'_\alpha(\vec{k})|^2 = \frac{1}{f_\alpha^2 N^2}\left[\left(\sum_{n=1}^{N} f_\alpha \cos(\vec{k}\cdot\vec{r}_n)\right)^2 + \left(\sum_{n=1}^{N} f_\alpha \sin(\vec{k}\cdot\vec{r}_n)\right)^2\right] \tag{7}$$

This quantity will be strictly equal to 1 only for a perfect crystal at 0 K and for $\vec{k}$ being a reciprocal vector of the lattice (fcc lattice in the case of UO_2).

Evaluations of $|S'_\alpha(\vec{k})|^2$ for solid UO_2 at 3000 K provide values comprised between 0.7 and 0.8 in the case of U atoms and less, between 0.3 and 0.4, for the O atoms because of their higher mobility (due to their lower mass). The increase of mobility above ≈2300–2600 K was often reported in previous simulations of UO_2 [4,13,18,12], our results confirm the observations of Walker [4] and Lindan and Gillan [18] that despite their mobility, oxygen atoms remain ordered.

When the liquid phase is considered, $|S'_\alpha(\vec{k})|^2$ is very close to 0 (less than 0.02) for both sublattices. This is illustrated on Fig. 3 for solid and liquid UO_2. The evolution of $|S'_U(\vec{k})|^2$ with time for the system of Fig. 2 is plotted on Fig. 4 for different initial temperatures. The identification of a solid phase or a liquid phase is quite straightforward.

2.3.2. Characteristics of the MD runs

For reasons discussed in Section 1, the melting problem has was studied considering only rigid ion potentials. Both MD codes GULP and Moldy [23] can therefore be consid-

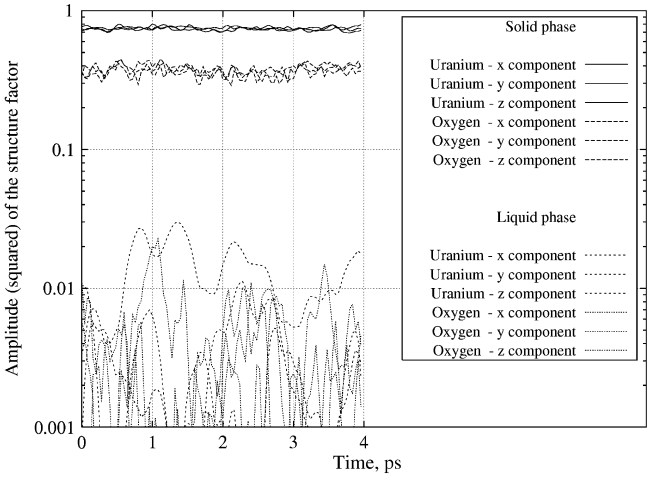

Fig. 3. Evolution of the amplitude of the structure factor with time, at 3000 K, for the solid and liquid phases.

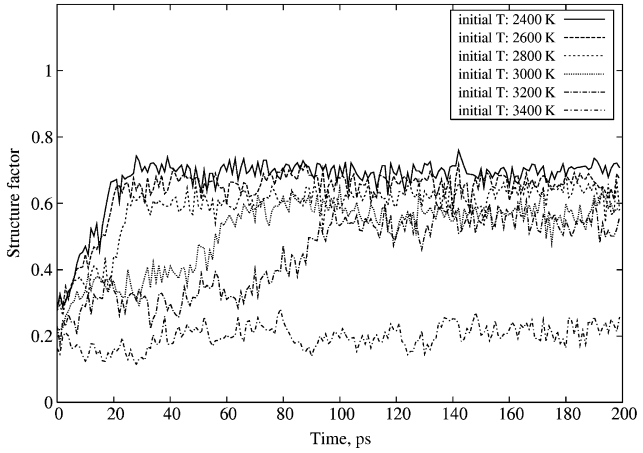

Fig. 4. Evolution of the amplitude of the Structure factor for the U sublattice – *Basak* potential. Solidification appears for the runs below 3200 K, it can be noted that the system can stay for a while with two phases (80 ps at 3200 K) before complete solidification. At 3400 K the two phase still coexist after 200 ps, in the same proportion as initially, as is can be seen during the run visualization or noting the conservation of the structure factor; longer simulations will probably finally favorise one phase because of the energy cost to maintain an interface.

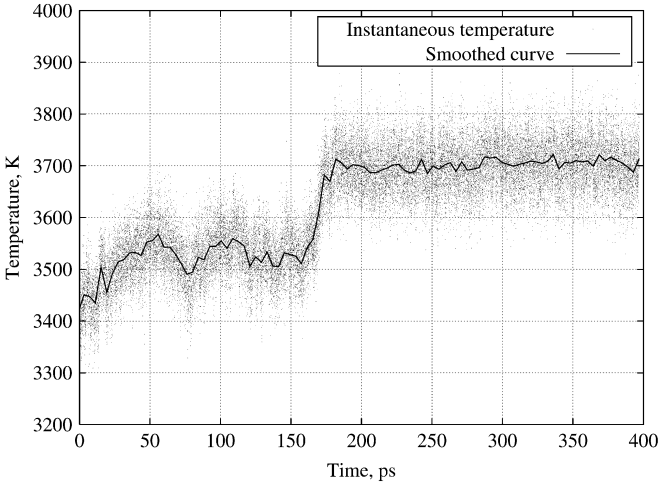

Fig. 5. Smoothing of the instantaneous temperature curve with a bezier curve.

ered. We preferred to perform the MD simulations with Moldy because Moldy allows to work at constant stress and energy while maintaining the angles of the simulation box at 90° (NPH ensemble), which is needed for simulations of a liquid phase. In addition Moldy is more efficient for large systems regarding the computing time.

The NPH ensemble was preferred to the NPT ensemble. Indeed imposing the temperature during the whole system equilibration time implies that the final state of the system consists of only one phase except when the system is *exactly* at the melting temperature, at least macroscopically. When the system energy is imposed, it is possible, because of the latent heat, to stay in the energy range where the melting proceeds. In that case both phases will coexist. For very small systems, like those used in MD, it is probably energetically more favorable to have only one phase, but the timescale to reach this state can become very long, as can be seen e.g. on Fig. 10.

The system we simulated consisted of a $5 \times 5 \times 5$ conventional unit cell solid phase system joined to a liquid phase system having the same physical dimension since the dimension of the contact face must be the same in order to apply periodic boundary conditions.

The temperature was controlled during the first 0.4 ps by a velocity rescaling procedure (to let the atoms at the interface equilibrate removing their excess energy), then the run proceeded at constant energy for 200 ps. The timestep of the simulations was 2 fs.

As the runs sample the NPH ensemble, the final temperature of the run is not imposed. It is difficult to provide one value per run as temperature fluctuations are inherent to the dynamics of finite-size systems. Only the average value of the 'instantaneous' temperature has a physical meaning. However when looking carefully at our simulations we could observe that, near the melting temperature, supplementary (occurring on larger time-scales) variations of temperature occured. In order to damp the rapid fluctuations of temperature, the temperature curve has been smoothed (in our case with bezier curves, see Fig. 5) and we will provide the minimum and maximum of this smoothed curve over the equilibrated part of the simulation. These variations are also given in the case where only one phase is present, in order to appreciate the supplementary variations of amplitude when two phases coexist. These larger fluctuations of temperature (observable during the first 180 ps of the run illustrated on Fig. 5) occur at the same time as the solid–liquid interface is moving.

2.3.3. Sensitivity

A test of sensitivity to the ensemble used and to the system pressure was made with NVE simulations of the system for different volumes imposed; and another one to the box size have been made in order to assess the intrinsic validity of our results. It appears that a variation of +10% of the liquid phase length, keeping the same number of atoms, results in a decrease of the system pressure to −1.5 GPa, and a decrease of 250–400 K of the predicted melting temperature. Also a large void region was formed (to compensate for the created empty space) around which many point defects could be found, as illustrated on Fig. 6.

The second test concerns the sensitivity of the predicted temperature to the size of the system. We did not expect to obtain different predictions of the melting temperature, but rather to observe a different behaviour of the interface. Indeed for the smallest systems the ratio of the energy of the separation surface per atom can be quite high and the system will naturally tend to favour the growth of one of the phases. For larger systems, the interfacial energy is relatively less important to the total energy of the system and the coexistence of liquid and solid UO_2 can become energetically possible. It also appeared that the simulations

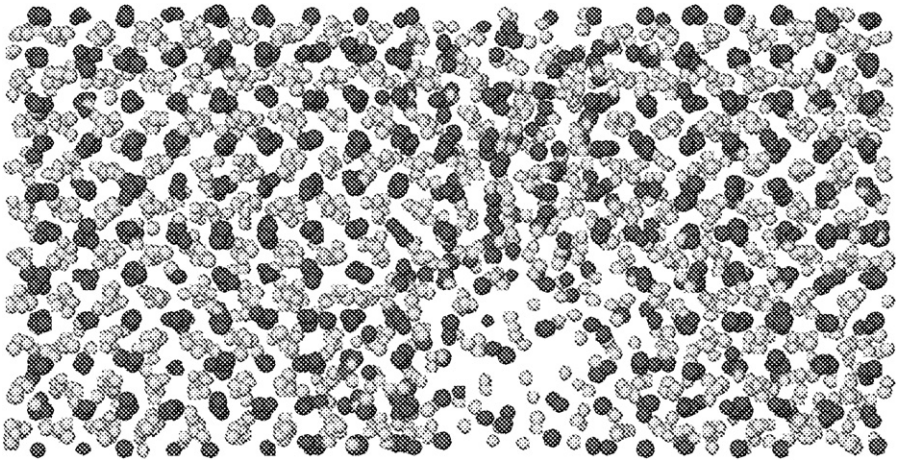

Fig. 6. Formation of a void during the solidification process when the volume is kept constant and larger than the volume at zero pressure. Picture obtained with the VMD program [22].

of large systems would require longer simulated times in order to achieve equilibration, particularly near the melting temperature. The choice of a ($5 \times 5 \times 5$ unit cells solid phase + liquid phase of an equivalent size) seems thus a good compromise in view of the accuracy of the results and the computing time.

The results of this sensitivity study can be found in Tables 1 and 2 for two of the potentials we considered: *Basak* and *Morelon*. The system sizes envisaged – because of the PBC the important parameter is the length in the x-direction, i.e. the thickness of the solid and liquid phase – consisted of $4 \times 4 \times 4$, $5 \times 5 \times 5$, $8 \times 8 \times 4$, $16 \times 8 \times 4$ and $20 \times 5 \times 5$ unit cells solid phase and a liquid phase of an equivalent size. These systems are, respectively, called 'small', 'normal', 'large', 'X-large' and 'XX-large'. They contain, respectively, 1344, 2625, 5376, 10 752 and 42 000 atoms.

Table 1
Sensitivity test to the box size – temperature (in K) range after equilibration

Initial temperature (K)	Box size		
	Small	Normal	Large
3000	*3455 ± 35*	*3300 ± 30*	*3450 ± 20*
3200	*3660 ± 30*	*3525 ± 25*	*3630 ± 15*
3400	*3810 ± 30*	**3540 ± 60**	**3540 ± 40**
3500	3400 ± 35	**3540 ± 60**	**3595 ± 35**
3600	3510 ± 20	3460 ± 20	3500 ± 20
3800	3660 ± 30	3635 ± 20	3650 ± 20

Calculations done with Moldy in the NPH ensemble, using the *Basak* potential. Bold data: coexistence of the solid and liquid phase, italic data: solidification of the system, normal data: liquefaction of the system.

3. Results

3.1. Lattice parameter evolution with temperature

Lattice parameter evolution with temperature has been computed for all potentials from 100 K to 3000 K and compared to the experimental curve proposed by Fink [24]. The comparison is plotted in Fig. 7. Three tendencies can be observed. A few potentials – *Arima2*, *Basak*, **Catlow2**, **Meis2**, *Morelon* – reproduce quite well the experimental curve, and its slope, up to 3000 K. All these potentials, with the exception of **Meis2**, are rigid ion potentials with non-formal charges. A second series of potentials – *Arima1*, **Catlow1**, **Grimes**, **Jackson1**, **Jackson2**, *Karakasi-*

Table 2
Sensitivity test to the box size – temperature (in K) range after equilibration

Initial temperature (K)	Box size				
	Small	Normal	Large	X Large	XX Large [a]
3000	*3425 ± 25*	*3340 ± 25*	*3350 ± 15*	*3280 ± 10*	*>3150*
3200	*3575 ± 25*	*3510 ± 20*	*3530 ± 25*	*3470 ± 5*	*>3220*
3400	*3765 ± 25*	*3625 ± 25*	**3520 ± 30**	**3500 ± 20**	3310 ± 5
3500	3290 ± 35	**3500 ± 70**	**3495 ± 50**	**3440 ± 40**	<3360
3600	3400 ± 30	3425 ± 20	**3540 ± 30**	**3530 ± 45**	<3435
3800	3580 ± 35	3570 ± 20	3500 ± 15	3565 ± 10	<3510

Calculations done with Moldy in the NPH ensemble, using the *Morelon* potential. Bold data: coexistence of the solid and liquid phase, italic data: solidification of the system, normal data: liquefaction of the system.

[a] For the largest system, stabilisation of temperature was generally not reached after 200 ps, therefore we provide the final temperature as upper (or lower) limit.

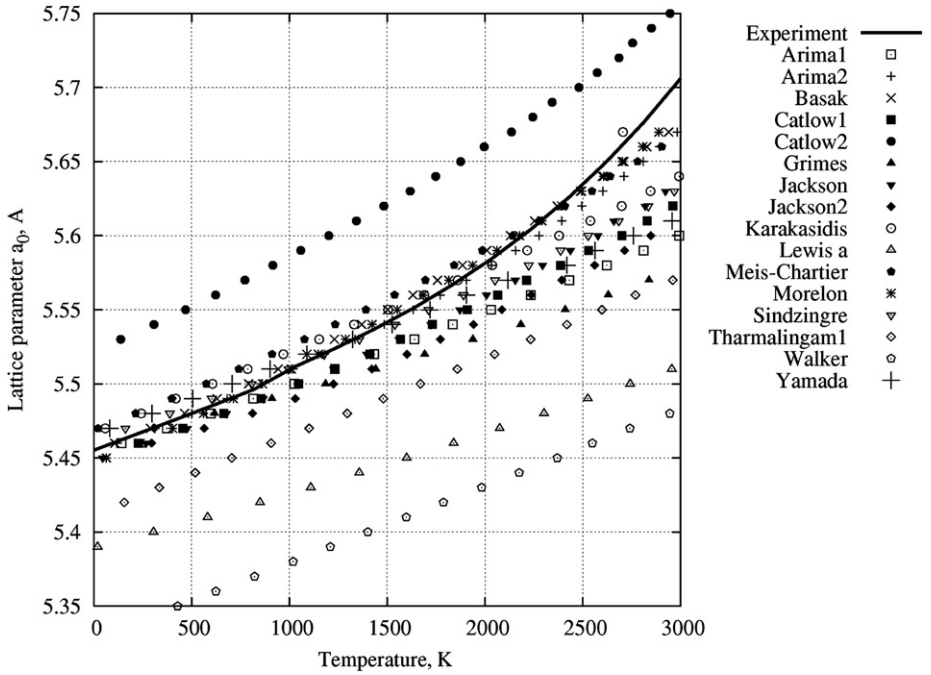

Fig. 7. Lattice parameter evolution with temperature for all potentials. Experimental curve from Fink [24]. In this and the following figures, crosses will be used for rigid ion potentials with non-formal charges, open symbols for rigid ion potentials with formal charges and full symbols for shell–core potentials.

dis, *Sindzingre*, *Tharmalingam1*, *Walker*, *Yamada* – could reproduce the good slope up to 2000 K, but do not reproduce well the anharmonic behaviour at higher temperatures. They also present a larger scatter for lattice parameter at 0 K [1]. These potentials are both rigid ion and shell–core potentials. The other potentials do not predict the correct slope – *Lewis_a* – or they could not be run at high temperatures, even with the addition of the repulsive term of Eq. (2) – **Busker**, **Lewis_b**, **Lewis_c**, *Tharmalingam2*. The coefficients used should perhaps be modified according to the strength of the attraction, but their adaptation for each problematic potential would have been very

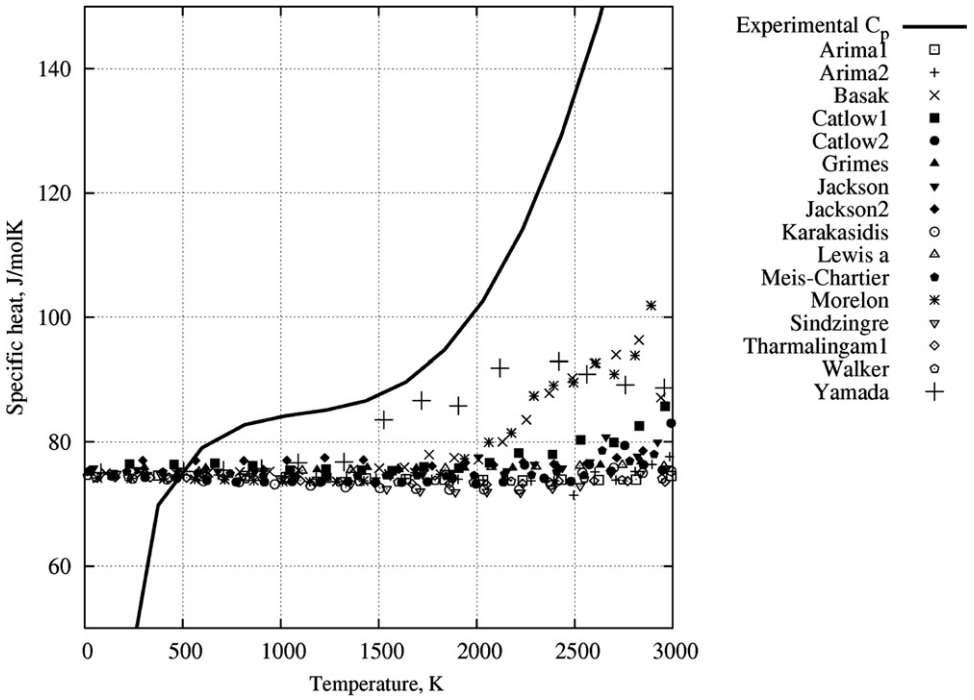

Fig. 8. Specific heat at constant volume evolution with temperature for all potentials. Experimental curve (at constant pressure) from Fink [24].

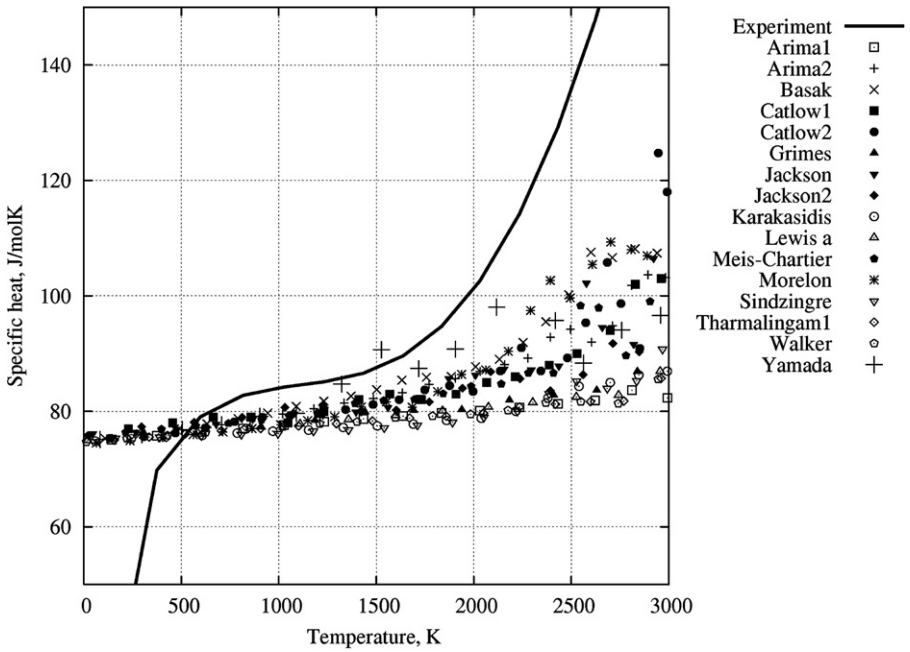

Fig. 9. Specific heat at constant pressure evolution with temperature for all potentials. Experimental curve from Fink [24].

time-consuming; we preferred to test the approach with a fixed set of coefficients and not to continue with those potentials where the approach failed.

3.2. Specific heat evolution with temperature

Specific heat at constant volume and constant pressure have been calculated, and compared to the experimental curve at constant pressure recommended by Fink [24]. The comparisons are, respectively, plotted in Fig. 8 (C_V) and Fig. 9 (C_p).

The estimation of C_V by all potentials is almost a constant and equal to the classical value of Dulong and Petit, over the whole temperature range. In the lower temperature region the predictions fail to reproduce the correct behaviour of C_V because the quantum mechanical aspects are not included in the classical molecular dynamics approach. The behaviour of specific heat at low temperature can, nevertheless, be determined from the phonon spectrum obtained from static calculations. At high temperatures, an increase of specific heat is observed for some potentials – mainly rigid ion potentials with non-formal charges, but also some shell–core potentials. This is explained (and visually confirmed) by the creation of temporary oxygen Frenkel pairs. It has also been suggested [25] that Schottky defects can contribute to the specific heat. This contribution cannot be modelled by MD because of the periodic boundary conditions: no surfaces exist to accommodate for the excess atoms.

The temperature evolution of specific heat at constant pressure is shown on Fig. 9. Since electronic excitation is also not taken into account by classical molecular dynamics, one may expect important difference between the experimental curve and the predictions of the potentials at elevated temperature. Apart from the potentials presenting oxygen Frenkel pairs formation, three tendencies can be observed on the graph. One category of potentials presents a large increase of C_p at high temperature. A second category is close to the previous one up to 2000 K, but the specific heat increase at higher temperature is less pronounced. The third category of potentials presents a too small increase of C_p over the whole temperature range.

These categories are exactly the same as mentioned for lattice parameter expansion (Section 3.1). This is evident if one considers the contribution to C_p from lattice expansion

$$C_p = C_V + 9\alpha^2 VT\beta_T \tag{8}$$

where α is the thermal expansion coefficient, V the molar volume, T the temperature and β_T the isothermal bulk modulus. The three categories correspond to the three different predictions of the thermal expansion coefficient α reported in Section 3.1.

3.3. Isothermal bulk modulus evolution with temperature

Isothermal bulk modulus evolution with temperature is reported on Fig. 10 and compared to the experimental curve determined by Martin [26]. Its behaviour is well reproduced by all potentials except the *Morelon* (that was fitted on defect properties) and *Sindzingre* potential. The **Grimes** potential whose parameters determination was theoretical overestimates the value of bulk modulus, as it was already observed in the static calculation part. However, the slope of the experimental curve is well reproduced by this potential. Most rigid ion potentials with non-formal

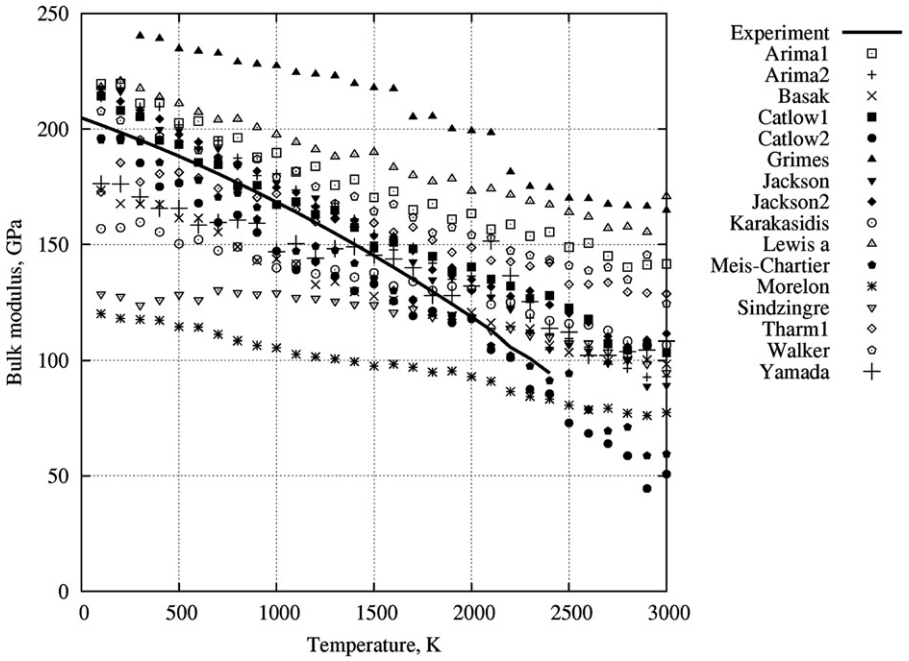

Fig. 10. Isothermal bulk modulus evolution with temperature for all potentials. Experimental curve from Martin [26].

charges were fitted to this type of curves, it is thus quite logical that they show the best agreement with experiments.

3.4. Gruneisen parameter evolution with temperature

Gruneisen parameter evolution with temperature is reported on Fig. 11. No experimental evolution of this parameter is provided for comparison, because we were unable to find experimental values of Gruneisen parameter evolution; and because at high temperature, electronic excitation would modify this parameter as for specific heat. The comparison shows that all potentials predict the same tendency, a slow decrease of this parameter with temperature. Only the *Arima2* potential predicts an almost constant value over the whole temperature range, and the *Yamada* potential shows a larger decrease at high temperature.

3.5. Melting temperature

The melting temperature has been computed for a few rigid ion potentials: *Basak*, *Karakasidis*, *Morelon*, *Walker* and *Yamada*. The shell–core potentials were discarded here

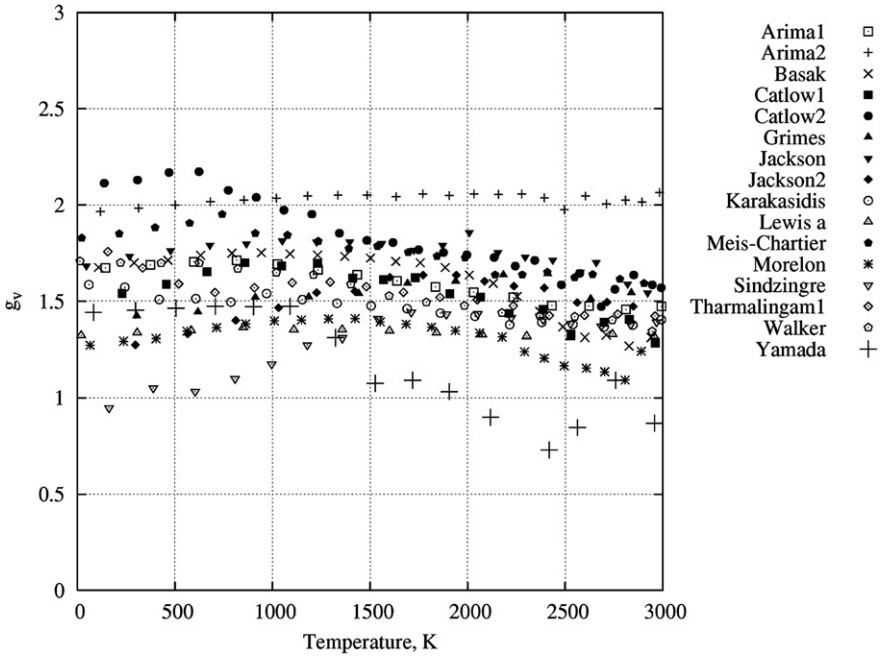

Fig. 11. Gruneisen parameter evolution with temperature for all potentials.

Table 3
Temperature (in K) range for the different potentials

Initial temperature	Potential				
	Basak [13]	*Karakasidis* [9]	*Morelon* [14]	*Walker* [4]	*Yamada* [12]
2800	*3140 ± 20*	*3035 ± 25*	*3145 ± 20*	*3070 ± 15*	*3135 ± 20*
3000	*3300 ± 30*	**3100 ± 50**	*3340 ± 25*	*3270 ± 25*	*3335 ± 20*
3050		**3145 ± 50**			
3100		**3170 ± 50**			
3150		**3205 ± 45**			
3200	*3525 ± 25*	3075 ± 25	*3510 ± 20*	**3360 ± 40**	*3525 ± 15*
3300	*3610 ± 25*		*3585 ± 20*		
3350	*3640 ± 25*		*3610 ± 20*		
3400	**3540 ± 65**	3220 ± 20	*3625 ± 25*	**3435 ± 45**	*3740 ± 20*
3450	**3540 ± 65**		*3710 ± 20*[a]	**3460 ± 45**	
3500	**3545 ± 60**		**3500 ± 65**	3350 ± 20	
3550	3440 ± 15		3320 ± 25	**3530 ± 50**	
3600	3460 ± 20	3430 ± 25	3425 ± 20	3400 ± 25	*3885 ± 25*
3800	3640 ± 20	3635 ± 20	3570 ± 20	3580 ± 25	*4065 ± 40*
4000	3880 ± 20	3840 ± 30	3810 ± 20	3520 ± 30	**4155 ± 55**
4100					4085 ± 30
4200					4195 ± 35
4300					4270 ± 25
4400					4360 ± 25
4500					4405 ± 25

Calculations done with Moldy in the NPH ensemble. Bold data: coexistence of the solid and liquid phase, italic data: solidification of the system, normal data: liquefaction of the system.

[a] In a first time, an equilibrium of the two phases was observed, for which the temperature range was 3520 ± 45 K.

because the computing time they require would have been too long. We proceeded by varying the initial temperature of the simulations and looking (by visualisation of the atoms trajectory and computing the structure factor amplitude) which state is reached by the system after 200 ps. As argued in the previous section, we report in Table 3 the range of variation of the smoothed curve of temperature, once it became visually stable. These predictions have to be compared to the experimental value of 3150 ± 20 K for $UO_{2.00}$ [27]. For some runs (*Karakasidis* potential with an initial temperature of 3000–3150 K and *Walker* potential with an initial temperature of 3200 K) it was not clear whether an equilibrium was reached at the end of the simulation or not. It is possible that a longer simulation would end with a solidification of the box.

4. General discussion

The combination of energy minimisation (see [1]) and molecular dynamics simulation provides information on the equilibrium and non-equilibrium properties of the potentials. It appeared from the static calculations that lattice properties (lattice parameter, elastic properties) are quite well reproduced by all potentials, mainly because potentials were fitted to these data. This fitting seems thus sufficient to reproduce the width and depth of the energy well around an atom in its regular lattice position The MD simulations provide information on the anharmonicity of the potentials, through the thermal expansion coefficient and specific heat evolution. Finally the various defect energies provide information and an evaluation of the interatomic potential when atoms are very far from their regular lattice position.

Lattice parameter expansion and specific heat evolution show that the potentials reproducing the best the anharmonicity are rigid ion models with non-formal charges – *Arima2*, *Basak*, *Morelon* – and some shell–core potentials – **Catlow2**, **Meis2**. Specific heat at constant volume indicates which potentials predict the apparition of oxygen Frenkel pairs with an increase of this value at high temperature. The potentials for which the largest increase of C_V is observed are again all rigid ion potentials with non-formal charges (including this time the *Yamada* potential); other potentials also predict oxygen Frenkel pair formation, but to a lesser extent: **Catlow1**, **Jackson1**, **Jackson2**. There is no direct one-to-one relationship between the Frenkel pair formation energy (derived in [1]) and the calculated Frenkel pair density in MD runs at elevated temperature. It is, however, possible that the oxygen Frenkel pair formation energy is lowered at high temperatures for some of the potentials because of lattice expansion and/or thermal agitation.

All potentials yield generally coherent results for bulk modulus and Gruneisen parameter evolution. Two potentials slightly overestimated or underestimated bulk modulus in static calculations. In the MD simulations it appeared that the **Grimes** potential could, nevertheless, reproduce the slope of bulk modulus evolution with temperature, which was not the case for the *Morelon* potential.

The simulations of the coexistence of the liquid and solid phases showed that the rigid ion potentials used for these simulations (*Basak*, *Karakasidis*, *Morelon*, *Walker* and

Yamada) predict quite accurately the melting temperature. The *Karakasidis* potential presents the best agreement; the *Basak*, *Morelon* and *Walker* potentials overpredict this value by 300–400 K. Only the *Yamada* potential seems to overpredict the melting temperature by a larger value, of about 900 K. Our simulations considered atoms only in the charge states +4 and −2 for, respectively, U and O atoms. Electronic excitations that would normally appear under the form of U^{3+} and U^{5+} ions cannot be considered in MD simulations (except by manually adding those atoms, but the electrons and holes will not be able to jump from one site to the other site). Their presence would increase the local disorder and it is expected that the inclusion of such effect would reduce the predicted melting temperature.

Our study indicates that rigid ion potentials with non-formal charges provide the best agreement with experimental data, and that they can reproduce the anharmonicity of the real material. These potentials were generally fitted on this type of curve, while shell–core potentials were generally developed in order to reproduce static properties. Anharmonicity effects are thus not included in the fitting procedure. However rigid ion potentials with non-formal charges are not the best choice under every circumstances:

- A study of Phillpot et al. [28] which compared the predictions of the *Yamada* and **Grimes** potentials with regard to thermal conductivity lead to a more mixed conclusion. In his study the *Yamada* potential showed a better reproduction of lattice parameter evolution compared to the **Grimes** potential, in agreement with our study, but with regard to thermal conductivity, the anharmonic behaviour was better reproduced by the **Grimes** potential.
- Difficulties will be encountered with rigid ion potentials when considering charged defects and charged impurities. In the case of charged defects, the results obtained in the first part of this work [1] indicated the importance of maintaining local electroneutrality by modifying the charge of the surrounding uranium atoms, creating localized electron or holes. The problem is: do the charge attributed to these localized electrons or holes, or more generally to any foreign atom introduced in the lattice, have to be considered as having the same ionicity fraction as the regular U or O atoms, or as having another ionicity fraction. In this perspective the use of formal charges seems to be necessary.

5. Conclusions

This work based on molecular dynamics simulations completes the comparison of interatomic developed for UO_2 made with static calculations in order to assess their range of applicability. We have computed the evolution of different thermodynamic properties – lattice parameter, specific heat, bulk modulus and Gruneisen parameter – as a function of temperature, for all potentials available in the literature. For some of the potentials we also computed the melting temperature. It appeared from this study that there is no 'universally good' potentials.

Rigid ion potentials with non-formal charges generally predict the best agreement with experiment, both in terms of static and dynamic calculations. This can be, at least partly, explained by the fitting of these potentials on thermal evolution curves rather than on elastic properties at low temperatures. Some shell–core potentials also show good results. The drawback of potentials with non-formal charges will appear when considering charged defects (including impurities) since it raises the problem of assuming (or not) the same ionicity of the defect and of the matrix.

In these perspectives, potentials with formal charges seem easier to handle.

The choice of a potential is thus a difficult compromise between its range of applicability based on the different results shown and its 'physically acceptable' applicability.

Acknowledgements

K.G. would like to thank SCK-CEN and ULB for his actual PhD grant.

References

[1] K. Govers, S. Lemehov, M. Hou, M. Verwerft, J. Nucl. Mater. 366 (2007) 161.
[2] K. Tharmalingam, Philos. Mag. 23 (1971) 199.
[3] C.R.A. Catlow, Proc. R. Soc. Lond. A 353 (1977) 533.
[4] J.R. Walker, C.R.A. Catlow, J. Phys. C: Solid State Phys. 14 (1981) L979.
[5] R.A. Jackson, C.R.A. Catlow, J. Nucl. Mater. 127 (1985) 161.
[6] G.V. Lewis, C.R.A. Catlow, J. Phys. C: Solid State Phys. 18 (1985) 1149.
[7] P. Sindzingre, M.J. Gillan, J. Phys. C: Solid State Phys. 21 (1988) 4017.
[8] R.W. Grimes, C.R.A. Catlow, Philos. Trans. R. Soc. Lond. A 335 (1991) 609.
[9] T. Karakasidis, P.J.D. Lindan, J. Phys.: Condens. Mat. 6 (1994) 2965.
[10] C. Meis, J.D. Gale, Mater. Sci. Eng. B 57 (1998) 52.
[11] M. Abramowski, R.W. Grimes, S. Owens, J. Nucl. Mater. 275 (1999) 12.
[12] K. Yamada, K. Kurosaki, M. Uno, S. Yamanaka, J. Alloy. Compd. 307 (2000) 10.
[13] C.B. Basak, A.K. Sengupta, H.S. Kamath, J. Alloy. Compd. 360 (2003) 210.
[14] N.-D. Morelon, D. Ghaleb, J.-M. Delhaye, L. Van Brutzel, Philos. Mag. 83 (13) (2003) 533.
[15] T. Arima, S. Yamasaki, Y. Inagaki, K. Idemitsu, J. Alloy. Compd. 400 (2005) 43.
[16] C. Meis, A. Chartier, J. Nucl. Mater. 341 (2005) 25.
[17] B.G. Dick, A.W. Overhauser, Phys. Rev. 112 (1958) 90.
[18] P.J.D. Lindan, M.J. Gillan, Philos. Mag. B 69 (3) (1994) 535.
[19] Private communication of T. Karakasidis, 2004.
[20] J.D. Gale, A.L. Rohl, Mol. Simul. 29 (2003) 291.
[21] M.P. Allen, D.J. Tildesley, Computer Simulation of Liquids, Clarendon, Oxford, 1987.
[22] W. Humphrey, A. Dalke, K. Schulten, J. Mol. Graphics 14 (1) (1996) 33.

[23] K. Refson, Comput. Phys. Commun. 126 (2000) 310.
[24] J.K. Fink, J. Nucl. Mater. 279 (2000) 1.
[25] Donald R. Olander, Fundamental Aspects of Nuclear Fuel Elements, Technical Information Center, Energy Research and Development Administration, 1976.
[26] D.G. Martin, High Temp. – High Press. 21 (1989) 13.
[27] D. Manara, C. Ronchi, M. Sheindlin, M. Lewis, M. Brykin, J. Nucl. Mater. 342 (2005) 148.
[28] S. Phillpot, T. Watanabe, P. Shukla, S. Sinnitt, J. Nino, J. Tulenko, R. Grimes, MMSNF-5 Workshop, Nice (France), 2006.